A Study of Supersonic Turbulence in Stagnating Plasma

E. Stambulchik, E. Kroupp, A. Starobinets,
D. Osin, V. I. Fisher, D. Alumot, and Y. Maron[1]
S. Davidovits and N. J. Fisch[2]
A. Fruchtman[3]

[1]Weizmann Institute of Science, Rehovot 7610001, Israel
[2]Princeton University, Princeton, New Jersey 08540, USA
[3]H.I.T.—Holon Institute of Technology, Holon 5810201, Israel

11th Serbian Conference on Spectral Line Shapes in Astrophysics
Šabac, Serbia
August 21–25, 2017

How Z-pinch works

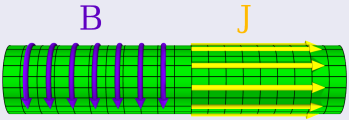

The $\vec{J} \times \vec{B}$ Lorentz force makes the plasma implode.

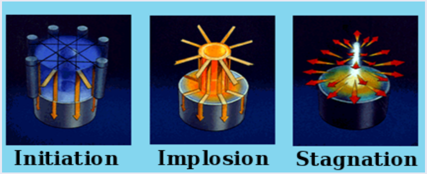

Most of the X-ray emission takes place at the stagnation phase.

How Z-pinch works

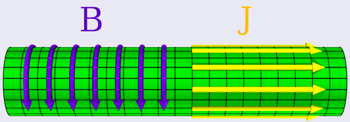

The $\vec{J} \times \vec{B}$ Lorentz force makes the plasma implode.

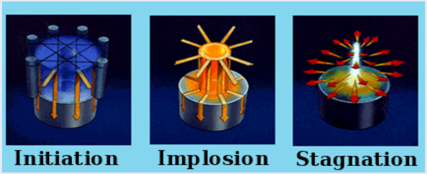

Most of the X-ray emission takes place at the stagnation phase.

"Z machine" (Sandia Labs, US)

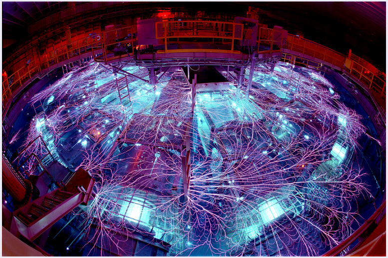

Z-pinch in Weizmann Inst. (Israel)

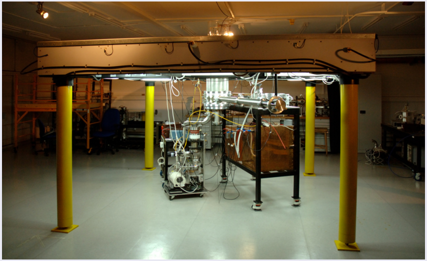

Pinches as laboratory astrophysics

Physics ABOUT BROWSE PRESS COLLECTIONS

Focus: Plasma Jets on Earth

August 2, 2005 • *Phys. Rev. Focus* 16, 4

A simple arrangement of electric and magnetic fields causes plasma to form shapes reminiscent of the jets generated near supermassive black holes.

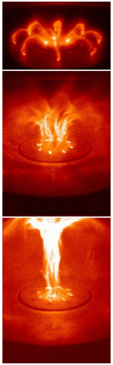

Phys. Rev. Lett. 95, 045002 (2005)

[You et al., 2005]

"A simple arrangement of electric and magnetic fields causes plasma to form shapes reminiscent of the jets generated near supermassive black holes."

Pinching is a naturally occuring phenomenon, but importance of z-pinches as an astrophysical laboratory goes well beyond that.

Pinches as laboratory astrophysics: im/explosions

Z-pinch ($r \sim 1$ cm)

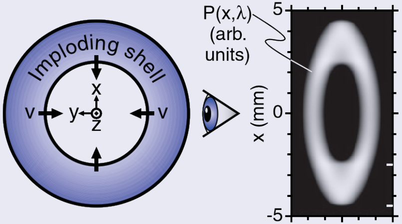

[Foord et al., 1994]

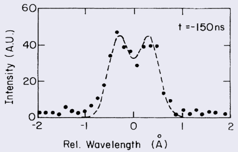

FIG. 2. A typical O III line profile ($\lambda_0 = 3047.1$ Å measured radially at $z = 11$ mm and $t' = -150$ ns. Redshifted and blueshifted components from each side of the annulus are observed. Doppler shifts correspond to a radial velocity ≈ 3 cm/μs.

Pinches as laboratory astrophysics: im/explosions

Z-pinch ($r \sim 1$ cm)

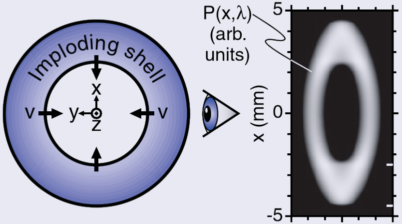

[Foord et al., 1994]

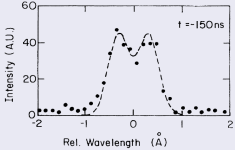

FIG. 2. A typical O III line profile ($\lambda_0 = 3047.1$ Å measured radially at $z = 11$ mm and $t' = -150$ ns. Redshifted and blueshifted components from each side of the annulus are observed. Doppler shifts correspond to a radial velocity ≈ 3 cm/μs.

NGC 7662 ($r \sim 1$ ly)

[Osterbrock et al., 1966]

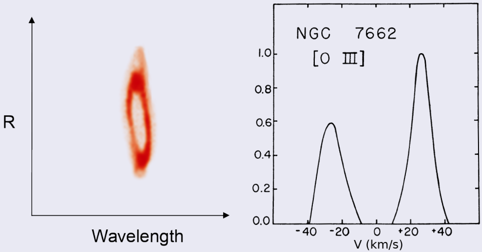

[Osin et al., 2011]

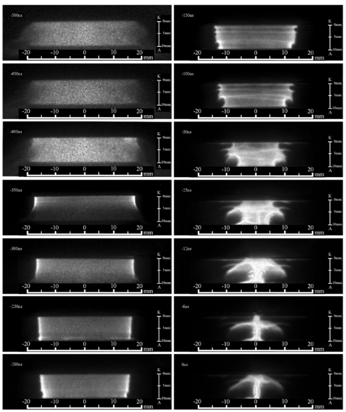

Rayleigh-Taylor instability produces “fingers” and filaments.

Pinches as laboratory astrophysics: instabilities

[Osin et al., 2011]

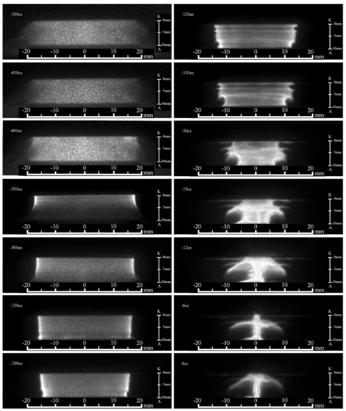

NGC 1952 (Crab Nebula)

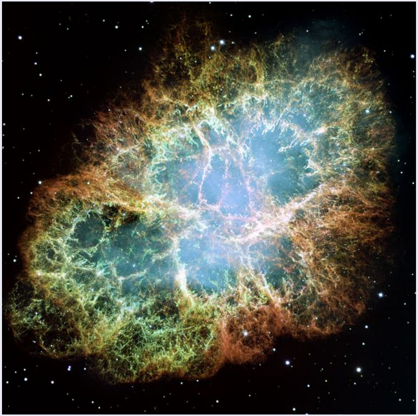

Rayleigh-Taylor instability produces “fingers” and filaments.

Energy conversion in imploding plasmas

Imploding plasmas are promising candidates for fusion (NIF, MagLIF) and unique sources of intense x-ray radiation (z-pinches).

NIF

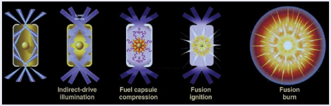

Z-pinch

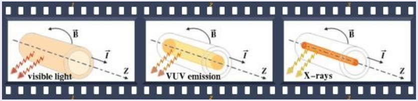

Conversion of hydrodynamic ion motion

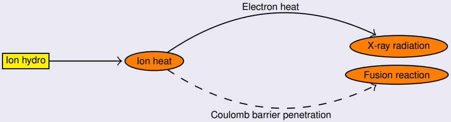

Thus, one needs to measure ion T_i. It is also important to know the hydro energy.

Principal difficulty:

The Doppler broadening (also, neutron spectrum) gives information only on the total ion velocity distribution $\rightarrow T_i^{\mathrm{eff}} \geq T_i$.

Importance of distinguishing between T_i^{eff} and T_i

Assuming $T_i = T_i^{\mathrm{eff}}$ may result in crucially misinterpreted data.

At WIS, we have succeeded developing advanced diagnostics capable of telling T_i^{eff} and T_i apart.

Diagnostics setup

Three time-resolved data sources: spectra of Ne Ly-α dielectronic satellites, gated x-ray pinhole imaging, and an absolutely calibrated photo-conductive detector (PCD) sensitive to $\hbar\omega \gtrsim 700\,\mathrm{eV}$.

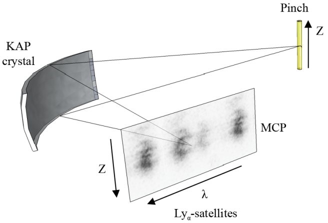

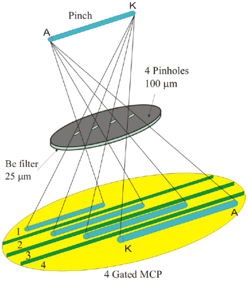

In addition, time-integrated wide spectrum is taken.

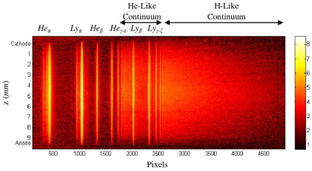

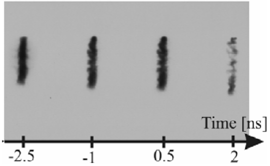

Plasma parameters inferred

Assuming the plasma is uniform, we obtain

- Plasma radius $r_{\rm pl}$ – from the pinhole x-ray imaging;

Plasma parameters inferred

Assuming the plasma is uniform, we obtain

- Plasma radius $r_{\rm pl}$ – from the pinhole x-ray imaging;
- Electron density n_e – from the satellite ratios;

Plasma parameters inferred

Assuming the plasma is uniform, we obtain

- Plasma radius r_{pl} – from the pinhole x-ray imaging;
- Electron density n_e – from the satellite ratios;
- Electron temperature T_e – from the time-dependent collisional-radiative (CR) model satisfying both the absolute PCD signal I_{PCD} and time-intergated continuum slope;

Plasma parameters inferred

Assuming the plasma is uniform, we obtain

- Plasma radius $r_{\rm pl}$ – from the pinhole x-ray imaging;
- Electron density n_e – from the satellite ratios;
- Electron temperature T_e – from the time-dependent collisional-radiative (CR) model satisfying both the absolute PCD signal $I_{\rm PCD}$ and time-intergated continuum slope;
- $T_i^{\rm eff}$ – from the satellite Doppler broadening (the Stark width is negligible);

Plasma parameters inferred

Assuming the plasma is uniform, we obtain

- Plasma radius r_{pl} – from the pinhole x-ray imaging;
- Electron density n_e – from the satellite ratios;
- Electron temperature T_e – from the time-dependent collisional-radiative (CR) model satisfying both the absolute PCD signal I_{PCD} and time-intergated continuum slope;
- T_i^{eff} – from the satellite Doppler broadening (the Stark width is negligible);

T_i is inferred from the data above, plus using either

- Detailed energy-balance analysis [Kroupp et al., 2011, Maron et al., 2013]; or
- Effect of Γ_{ii} on Stark lineshapes of high-n transitions [Alumot et al., 2017] (in preparation).

Plasma parameters inferred

Assuming the plasma is uniform, we obtain

- Plasma radius r_{pl} – from the pinhole x-ray imaging;
- Electron density n_e – from the satellite ratios;
- Electron temperature T_e – from the time-dependent collisional-radiative (CR) model satisfying both the absolute PCD signal I_{PCD} and time-intergated continuum slope;
- T_i^{eff} – from the satellite Doppler broadening (the Stark width is negligible);

T_i is inferred from the data above, plus using either

- Detailed energy-balance analysis [Kroupp et al., 2011, Maron et al., 2013]; or
- Effect of Γ_{ii} on Stark lineshapes of high-n transitions [Alumot et al., 2017] (in preparation).

This modeling described all the data very well, within 1 – 2 std. dev.

Determination of n_e and T_i^{eff}

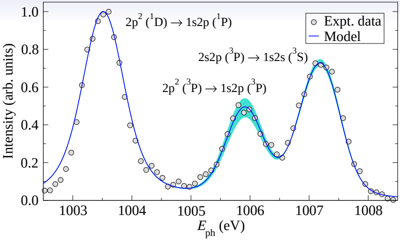

Widths and intensities of the Ne Ly-α satellites allow for determining T_i^{eff} and n_e, respectively. In this example, $T_i^{\mathrm{eff}} = 1200\,\mathrm{eV}$ and $n_e = (5 \pm 1) \times 10^{20}\,\mathrm{cm}^{-3}$.

Determination of n_e and $T_i^{\rm eff}$

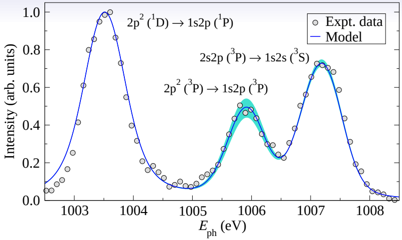

Widths and intensities of the Ne Ly-α satellites allow for determining $T_i^{\rm eff}$ and n_e, respectively. In this example, $T_i^{\rm eff} = 1200\,{\rm eV}$ and $n_e = (5 \pm 1) \times 10^{20}\,{\rm cm}^{-3}$.

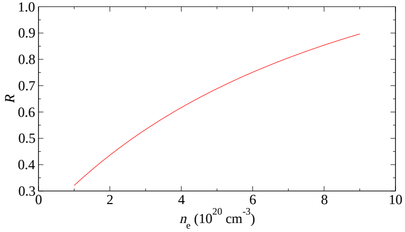

$I_{2p^2(^3P)\rightarrow 1s2p(^3P)}/I_{2s2p(^3P)\rightarrow 1s2s(^3S)}$ intensity ratio R is sensitive to n_e but practically independent of T_e [Seely, 1979, Kroupp et al., 2007].

Determination of T_i during z-pinch stagnation

Two methods have been used:

1. Detailed energy-balance analysis

$$\frac{T_i - T_e}{\tau_{ie}} = \frac{dT_i^{\mathrm{eff}}}{dt}$$

[Kroupp et al., 2011]

2. Effect of Γ_{ii} on Stark lineshapes

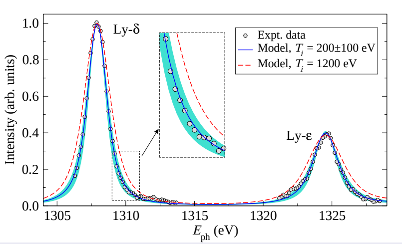

[Alumot et al., 2017] (in preparation)

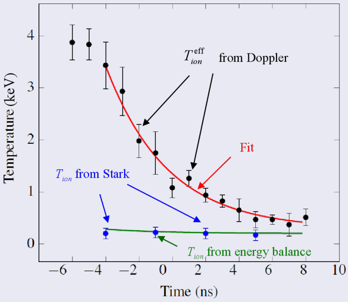

Both methods give the same, consistent results.

Hypothesis: turbulent hydromotion

It was inferred that, at the stagnation phase,

- the ion kinetic energy at the stagnation phase is dominantly stored in non-thermal hydrodynamic motion;

Hypothesis: turbulent hydromotion

It was inferred that, at the stagnation phase,

- the ion kinetic energy at the stagnation phase is dominantly stored in non-thermal hydrodynamic motion;
- the plasma appeared largely uniform at spatial and temporal scales down to $\sim 100\,\mu\mathrm{m}$ and $\sim$1 ns, respectively;

Hypothesis: turbulent hydromotion

It was inferred that, at the stagnation phase,

- the ion kinetic energy at the stagnation phase is dominantly stored in non-thermal hydrodynamic motion;
- the plasma appeared largely uniform at spatial and temporal scales down to $\sim 100\,\mu\mathrm{m}$ and ~1 ns, respectively;
- the Reynolds number is high ($\sim 10^5$);

Hypothesis: turbulent hydromotion

It was inferred that, at the stagnation phase,

- the ion kinetic energy at the stagnation phase is dominantly stored in non-thermal hydrodynamic motion;
- the plasma appeared largely uniform at spatial and temporal scales down to $\sim 100\,\mu\mathrm{m}$ and $\sim$1 ns, respectively;
- the Reynolds number is high $(\sim 10^5)$;
- the flow is supersonic.

Hypothesis: turbulent hydromotion

It was inferred that, at the stagnation phase,

- the ion kinetic energy at the stagnation phase is dominantly stored in non-thermal hydrodynamic motion;
- the plasma appeared largely uniform at spatial and temporal scales down to $\sim 100\,\mu\mathrm{m}$ and ~1 ns, respectively;
- the Reynolds number is high $(\sim 10^5)$;
- the flow is supersonic.

Turbulence is an obvious candidate for such a significant small-scale hydrodynamic motion.

Hypothesis: turbulent hydromotion

It was inferred that, at the stagnation phase,

- the ion kinetic energy at the stagnation phase is dominantly stored in non-thermal hydrodynamic motion;
- the plasma appeared largely uniform at spatial and temporal scales down to $\sim 100\,\mu\mathrm{m}$ and $\sim$1 ns, respectively;
- the Reynolds number is high $(\sim 10^5)$;
- the flow is supersonic.

Turbulence is an obvious candidate for such a significant small-scale hydrodynamic motion.

Were supersonic turbulence present, it would imply substantial nonuniformity in quantities such as the density. However, the previous analysis assumed a uniform plasma.

New analysis

The data need to be re-analyzed assuming a physically sound model of turbulence. [Kroupp et al., 2017]

Instead of $n_e = n_e^0 = \mathrm{const}$, there is now a probability distribution function (PDF) $P(n_e)$ – actually, $P(t, z; n_e)$.

New analysis

The data need to be re-analyzed assuming a physically sound model of turbulence. [Kroupp et al., 2017]

Instead of $n_e = n_e^0 = \mathrm{const}$, there is now a probability distribution function (PDF) $P(n_e)$ – actually, $P(t, z; n_e)$.

Let us switch to dimensionless quantity

$$\xi \equiv n_e/n_e^0; \int P(\xi)\,\mathrm{d}\xi = 1.$$

The average density is

$$\langle n_e \rangle = n_e^0 \int \xi\, P(\xi)\,\mathrm{d}\xi.$$

(note that $\langle n_e \rangle \neq n_e^0$).

New analysis (cont.)

Assuming the collisional-radiative equilibrium is established much faster than the hydromotion, the intensity of a spectral line (or continuum radiation) is [Stamm et al., 2017]

$$\langle I \rangle = \int \alpha(\vec{r}) d^3 r = \pi r_{\mathrm{pl}}^2 \ell \int \alpha(\xi) P(\xi)\, \mathrm{d}\xi,$$

where $\alpha \propto \xi^2$ is the local plasma emissivity, and r_{pl} and ℓ is the radius and length of the plasma segment, respectively.

New analysis (cont.)

Assuming the collisional-radiative equilibrium is established much faster than the hydromotion, the intensity of a spectral line (or continuum radiation) is [Stamm et al., 2017]

$$\langle I \rangle = \int \alpha(\vec{r}) d^3 r = \pi r_{\rm pl}^2 \ell \int \alpha(\xi) P(\xi)\, {\rm d}\xi,$$

where $\alpha \propto \xi^2$ is the local plasma emissivity, and $r_{\rm pl}$ and ℓ is the radius and length of the plasma segment, respectively.

In particular, the *absolutely calibrated* PCD signal is

$$I_{\rm PCD} \propto \pi r_{\rm pl}^2 \ell \int \xi^2 P(\xi)\, {\rm d}\xi.$$

New analysis (cont.)

Assuming the collisional-radiative equilibrium is established much faster than the hydromotion, the intensity of a spectral line (or continuum radiation) is [Stamm et al., 2017]

$$\langle I\rangle = \int \alpha(\vec{r})d^3r = \pi r_{\mathrm{pl}}^2 \ell \int \alpha(\xi)P(\xi)\,\mathrm{d}\xi,$$

where $\alpha \propto \xi^2$ is the local plasma emissivity, and r_{pl} and ℓ is the radius and length of the plasma segment, respectively.

In particular, the *absolutely calibrated* PCD signal is

$$I_{\mathrm{PCD}} \propto \pi r_{\mathrm{pl}}^2 \ell \int \xi^2 P(\xi)\,\mathrm{d}\xi.$$

$$\left(1 - \frac{\delta I_{\mathrm{PCD}}}{I_{\mathrm{PCD}}}\right)\left(\frac{r_{\mathrm{pl}}^0}{r_{\max}}\right)^2 \le \int \xi^2\, P(\xi)\,\mathrm{d}\xi \le \left(1 + \frac{\delta I_{\mathrm{PCD}}}{I_{\mathrm{PCD}}}\right)\left(\frac{r_{\mathrm{pl}}^0}{r_{\min}}\right)^2 .$$

New analysis (cont.)

Density determination:

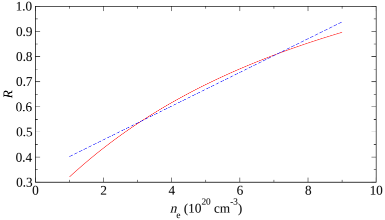

Use linearization

$R \approx R^0 + a_R(n_e/n_e^0 - 1)$, so

$$\langle R \rangle = R^0 + a_R \frac{\int (\xi - 1)\xi^2 P(\xi)\,\mathrm{d}\xi}{\int \xi^2 P(\xi)\,\mathrm{d}\xi}.$$

New analysis (cont.)

Density determination:

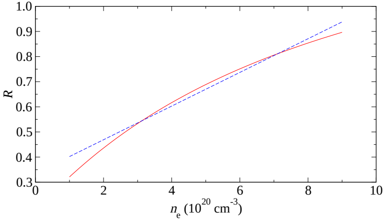

Use linearization
$R \approx R^0 + a_R(n_e/n_e^0 - 1)$, so

$$\langle R \rangle = R^0 + a_R \frac{\int (\xi - 1)\xi^2 P(\xi)\, d\xi}{\int \xi^2 P(\xi)\, d\xi}.$$

The measured quantity R_{expt} is known – and should remain – within its error bars, i.e., $\langle R \rangle = R_{\text{expt}} = R^0 \pm \delta R$. Therefore,

$$1 - \frac{\delta R}{a_R} \leq \frac{\int \xi^3 P(\xi)\, d\xi}{\int \xi^2 P(\xi)\, d\xi} \leq 1 + \frac{\delta R}{a_R}.$$

Constraints on $P(\xi)$

To summarize:

$$\left(1 - \frac{\delta I_{\mathrm{PCD}}}{I_{\mathrm{PCD}}}\right)\left(\frac{r_{\mathrm{pl}}^{0}}{r_{\max}}\right)^{2} \leq \int \xi^{2} P(\xi)\,\mathrm{d}\xi \leq \left(1 + \frac{\delta I_{\mathrm{PCD}}}{I_{\mathrm{PCD}}}\right)\left(\frac{r_{\mathrm{pl}}^{0}}{r_{\min}}\right)^{2} .$$

$$1 - \frac{\delta R}{a_R} \leq \frac{\int \xi^{3} P(\xi)\,\mathrm{d}\xi}{\int \xi^{2} P(\xi)\,\mathrm{d}\xi} \leq 1 + \frac{\delta R}{a_R} .$$

Constraints on $P(\xi)$

To summarize:

$$\left(1-\frac{\delta I_{\mathrm{PCD}}}{I_{\mathrm{PCD}}}\right)\left(\frac{r_{\mathrm{pl}}^0}{r_{\max}}\right)^2 \le \int \xi^2\, P(\xi)\, \mathrm{d}\xi \le \left(1+\frac{\delta I_{\mathrm{PCD}}}{I_{\mathrm{PCD}}}\right)\left(\frac{r_{\mathrm{pl}}^0}{r_{\min}}\right)^2 .$$

$$1-\frac{\delta R}{a_R} \le \frac{\int \xi^3 P(\xi)\, \mathrm{d}\xi}{\int \xi^2 P(\xi)\, \mathrm{d}\xi} \le 1+\frac{\delta R}{a_R} .$$

Once $P(\xi)$ is determined, the model plasma radius is corrected:

$$r_{\mathrm{pl}} = r_{\mathrm{pl}}^0 / \sqrt{\langle \xi^2 \rangle} .$$

Constraints on $P_V(\xi_V)$ and β

The last step is to use the volumetric density distribution:

$$\int P_V(\xi_V)\,\mathrm{d}\xi_V = 1, \int \xi_V P_V(\xi_V)\,\mathrm{d}\xi_V = 1.$$

Introduce $\beta \equiv \xi/\xi_V = \langle n_e \rangle / n_e^0$; so $\langle \xi^k \rangle = \beta^k \langle \xi_V^k \rangle$.

Constraints on $P_V(\xi_V)$ and β

The last step is to use the volumetric density distribution:

$$\int P_V(\xi_V)\,\mathrm{d}\xi_V = 1, \int \xi_V P_V(\xi_V)\,\mathrm{d}\xi_V = 1.$$

Introduce $\beta \equiv \xi/\xi_V = \langle n_e\rangle/n_e^0$; so $\langle \xi^k\rangle = \beta^k \langle \xi_V^k\rangle$.

Finally:

$$\sqrt{\frac{1-\frac{\delta I_{\mathrm{PCD}}}{I_{\mathrm{PCD}}}}{\langle\xi_V^2\rangle}\frac{r_{\mathrm{pl}}^0}{r_{\max}}} \le \beta \le \sqrt{\frac{1+\frac{\delta I_{\mathrm{PCD}}}{I_{\mathrm{PCD}}}}{\langle\xi_V^2\rangle}\frac{r_{\mathrm{pl}}^0}{r_{\min}}}$$

$$\left(1-\frac{\delta R}{a_R}\right)\frac{\langle\xi_V^2\rangle}{\langle\xi_V^3\rangle} \le \beta \le \left(1+\frac{\delta R}{a_R}\right)\frac{\langle\xi_V^2\rangle}{\langle\xi_V^3\rangle}$$

$$r_{\mathrm{pl}} = r_{\mathrm{pl}}^0/(\beta\sqrt{\langle\xi_V^2\rangle})$$

Turbulence density PDF

Volumetric PDF of [Hopkins, 2013]:

$$P_V(\xi_V)\,\mathrm{d}\xi_\mathrm{V} = \frac{\mathrm{I}_1\left(2\sqrt{\lambda\omega(\xi_V)}\right)}{\exp[\lambda + \omega(\xi_\mathrm{V})]}\sqrt{\frac{\lambda}{\theta^2\omega(\xi_V)}}\,\frac{\mathrm{d}\xi_\mathrm{V}}{\xi_\mathrm{V}}$$

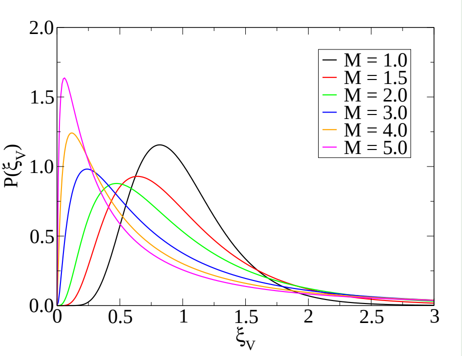

Here,

$\lambda \equiv (1+\theta)^{3/2}\ln\left(1+M_c^2\right)/2\theta^2$

$\omega(\xi_V) \equiv \lambda/(1+\theta) - \ln(\xi_\mathrm{v})/\theta$

$\theta \approx 0.05M_c$

Compressive Mach number

$M_c = bM,\ b \approx 0.4$

I_1 – modified Bessel function of the first kind

Constraints on $P_V(\xi_V)$ and β

The last step is to use the volumetric density distribution:

$$\int P_V(\xi_V)\,\mathrm{d}\xi_V = 1, \int \xi_V P_V(\xi_V)\,\mathrm{d}\xi_V = 1.$$

Introduce $\beta \equiv \xi/\xi_V = \langle n_e \rangle / n_e^0$; so $\langle \xi^k \rangle = \beta^k \langle \xi_V^k \rangle$.

Finally:

$$\sqrt{\frac{1 - \frac{\delta I_{\mathrm{PCD}}}{I_{\mathrm{PCD}}}}{\langle \xi_V^2 \rangle} \frac{r_{\mathrm{pl}}^0}{r_{\mathrm{max}}}} \leq \beta \leq \sqrt{\frac{1 + \frac{\delta I_{\mathrm{PCD}}}{I_{\mathrm{PCD}}}}{\langle \xi_V^2 \rangle} \frac{r_{\mathrm{pl}}^0}{r_{\mathrm{min}}}}$$

$$\left(1 - \frac{\delta R}{a_R}\right) \frac{\langle \xi_V^2 \rangle}{\langle \xi_V^3 \rangle} \leq \beta \leq \left(1 + \frac{\delta R}{a_R}\right) \frac{\langle \xi_V^2 \rangle}{\langle \xi_V^3 \rangle}$$

$$r_{\mathrm{pl}} = r_{\mathrm{pl}}^0 / (\beta \sqrt{\langle \xi_V^2 \rangle})$$

Results: model mean density and plasma radius

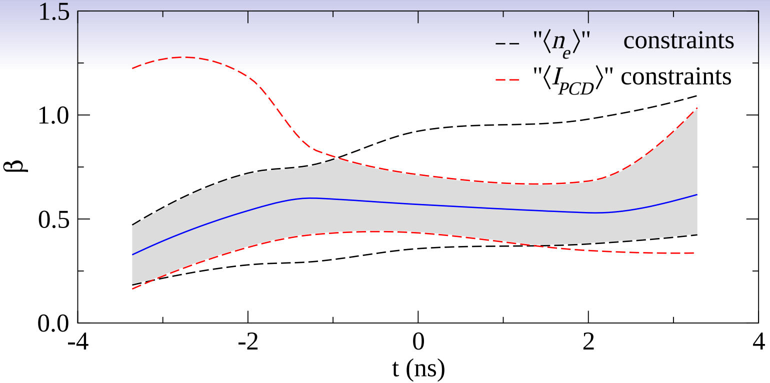

The mean plasma density is inferred to be lower by a factor ∼2.

Results: model mean density and plasma radius

The corrected plasma model radius fits the data better.

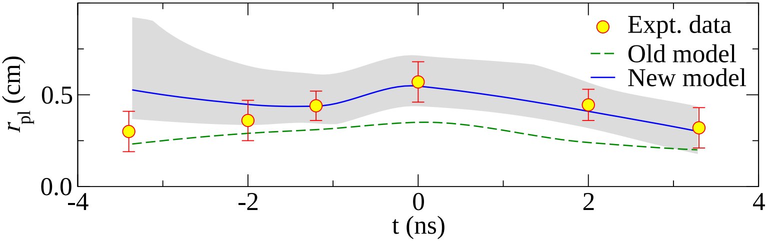

Results: model mean density and plasma radius

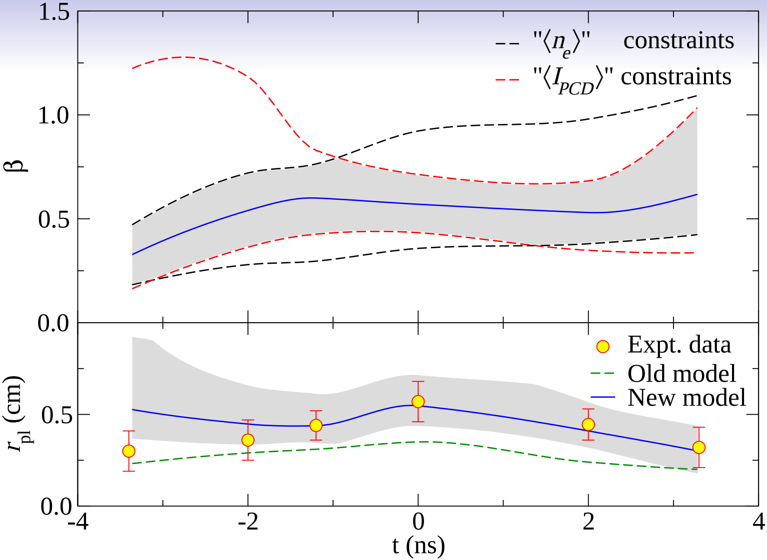

The other plasma parameters (T_e, T_i, and T_i^{eff}) remain unaffected.

Results in a wider scientific context

In addition to better understanding of z-pinch stagnation plasmas, a crucial question arises:

Is the supersonic turbulent hydromotion generated and carried along during the implosion phase?

Results in a wider scientific context

In addition to better understanding of z-pinch stagnation plasmas, a crucial question arises:

Is the supersonic turbulent hydromotion generated and carried along during the implosion phase?

If yes (and we have preliminary results confirming it), then z-pinches represent a test bed for:

- a recently proposed novel fast ignition scheme [Davidovits and Fisch, 2016] for inertial confinement;
- astrophysical phenomena, such as molecular cloud dynamics, star formation efficiency, the core mass/stellar initial mass function, and more.

Conclusions

- Inferred $T_i \ll T_i^{\rm eff}$ at z-pinch stagnation, with Re $\sim 10^5$ and observing no large-scale plasma non-uniformities, strongly hints at turbulence; supersonic one ($M \sim 1-2$).

Conclusions

- Inferred $T_i \ll T_i^{\mathrm{eff}}$ at z-pinch stagnation, with Re $\sim 10^5$ and observing no large-scale plasma non-uniformities, strongly hints at turbulence; supersonic one ($M \sim$ 1 – 2).
- Analysis with the uniform-plasma assumption lifted shows that the picture of a preponderance of turbulent energy remains intact.

Conclusions

- Inferred $T_i \ll T_i^{\mathrm{eff}}$ at z-pinch stagnation, with Re $\sim 10^5$ and observing no large-scale plasma non-uniformities, strongly hints at turbulence; supersonic one ($M \sim 1-2$).
- Analysis with the uniform-plasma assumption lifted shows that the picture of a preponderance of turbulent energy remains intact.
- As a result, the mean plasma density is inferred to be lower by a factor $\sim$2.

Conclusions

- Inferred $T_i \ll T_i^{\mathrm{eff}}$ at z-pinch stagnation, with Re $\sim 10^5$ and observing no large-scale plasma non-uniformities, strongly hints at turbulence; supersonic one ($M \sim 1 - 2$).
- Analysis with the uniform-plasma assumption lifted shows that the picture of a preponderance of turbulent energy remains intact.
- As a result, the mean plasma density is inferred to be lower by a factor $\sim$2.
- This turbulent-plasma model is not only consistent with the observations, it improves the agreement with them (r_{pl}).

Conclusions

- Inferred $T_i \ll T_i^{\mathrm{eff}}$ at z-pinch stagnation, with Re $\sim 10^5$ and observing no large-scale plasma non-uniformities, strongly hints at turbulence; supersonic one ($M \sim$ 1 – 2).
- Analysis with the uniform-plasma assumption lifted shows that the picture of a preponderance of turbulent energy remains intact.
- As a result, the mean plasma density is inferred to be lower by a factor ∼2.
- This turbulent-plasma model is not only consistent with the observations, it improves the agreement with them (r_{pl}).
- Beyond aiding our understanding of z-pinches, we hope this study can provide fertile ground for dealing with related problems of astrophysical interest.

Thank you!

Bibliography I

Alumot, D., Kroupp, E., Stambulchik, E., Maron, Y., and Fisher, A. (2017).
Determination of ion temperature in high-energy-density plasmas using the Stark effect.
In preparation.

Davidovits, S. and Fisch, N. J. (2016).
Phys. Rev. Lett., 116(10):105004.

Foord, M. E., Maron, Y., Davara, G., Gregorian, L., and Fisher, A. (1994).
Phys. Rev. Lett., 72:3827–3830.

Hopkins, P. F. (2013).
Mon. Not. R. Astron. Soc., 430(3):1880.

Kroupp, E., D. Osin, Starobinets, A., Fisher, V., Bernshtam, V., Maron, Y., Uschmann, I., Förster, E., Fisher, A., and Deeney, C. (2007).
Phys. Rev. Lett., 98:115001.

Kroupp, E., Osin, D., Starobinets, A., Fisher, V., Bernshtam, V., Weingarten, L., Maron, Y., Uschmann, I., Förster, E., Fisher, A., Cuneo, M. E., Deeney, C., and Giuliani, J. L. (2011).
Phys. Rev. Lett., 107:105001.

Kroupp, E., Stambulchik, E., Starobinets, A., Osin, D., Fisher, V. I., Alumot, D., Maron, Y., Davidovits, S., Fisch, N. J., and Fruchtman, A. (2017).
arXiv:1705.03114 [physics].
Submitted to Phys. Rev. Lett.

Maron, Y., Starobinets, A., Fisher, V. I., Kroupp, E., Osin, D., Fisher, A., Deeney, C., Coverdale, C., Lepell, P. D., Yu, E., Jennings, C., Cuneo, M. E., Herrmann, M. C., Porter, J. L., Velikovich, A., Mehlhorn, T., and Apruzese, J. P. (2013).
Phys. Rev. Lett., 111:035001.

Osin, D., Kroupp, E., Starobinets, A., Rosenzweig, G., Alumot, D., Maron, Y., Fisher, A., Yu, E., Giuliani, J. L., and Deeney, C. (2011).
Plasma Science, IEEE Transactions on, 39(11):2392–2393.

Osterbrock, D. E., Miller, J. S., and Weedman, D. W. (1966).
Astrophys. J., 145:697–707.

Seely, J. F. (1979).
Phys. Rev. Lett., 42:1606–1609.

Stamm, R., Hannachi, I., Meireni, M., Capes, H., Godbert-Mouret, L., Koubiti, M., Rosato, J., Marandet, Y., Dimitrijević, M., and Simić, Z. (2017).
Eur. Phys. J. D, 71(3):68.

Bibliography III

You, S., Yun, G. S., and Bellan, P. M. (2005).
Phys. Rev. Lett., 95(4):045002.

Zeldovich, Ya. B. and Raizer, Yu. (1967).
Physics of shock waves and high-temperature hydrodynamic phenomena.
Academic Press, New York.

Extra material

Data summary

The experimental data [Kroupp et al., 2011] relevant for the analysis presented; the plasma parameters assumed for ($r^0_{\rm pl}$, n^0_e, T_e) and inferred from (T_i, M, Re) the *uniform*-plasma modeling; the calculated isothermal turbulence parameters, volumetric density factor β and respectively corrected plasma electron density and radius. Units are as follows: all radii are in mm, all temperatures are in eV, and densities are in $10^{20}\,{\rm cm}^{-3}$.

Experimental data						Uniform plasma						Isothermal turbulence						
t (ns)	δR	$I_{\rm PCD}$ (GW)	$r_{\rm min}$	$r_{\rm max}$	$T_i^{\rm eff}$	$r^0_{\rm pl}$	n^0_e	T_e	T_i	M	Re	θ	$\sigma^2_{s,V}$	$\langle\xi^2_V\rangle$	$\langle\xi^3_V\rangle$	β	$n_e^{\rm turb}$	$r_{\rm pl}^{\rm turb}$
-3.4	0.15	0.35 ± 0.3	0.19	0.41	3000	0.23	6.0	120	250	2.4	8.1×10^4	0.048	0.70	1.84	5.77	0.32	1.9	0.53
-2.0	0.15	2.0 ± 1.0	0.25	0.47	2100	0.29	6.0	175	230	1.7	6.9×10^4	0.034	0.40	1.44	2.86	0.54	3.2	0.45
-1.2	0.15	3.8 ± 1.1	0.36	0.52	1800	0.31	6.0	190	210	1.6	7.7×10^4	0.032	0.36	1.39	2.60	0.60	3.6	0.44
0.0	0.15	6.5 ± 0.7	0.46	0.68	1300	0.35	6.0	185	200	1.3	8.9×10^4	0.026	0.25	1.26	1.96	0.57	3.4	0.55
2.0	0.15	3.6 ± 1.0	0.36	0.53	900	0.24	6.0	155	180	1.2	7.4×10^4	0.024	0.21	1.22	1.80	0.53	3.2	0.41
3.3	0.15	2.3 ± 0.9	0.21	0.43	720	0.20	6.0	140	180	1.0	5.1×10^4	0.020	0.15	1.16	1.53	0.62	3.7	0.30

Results: turbulent density PDF's

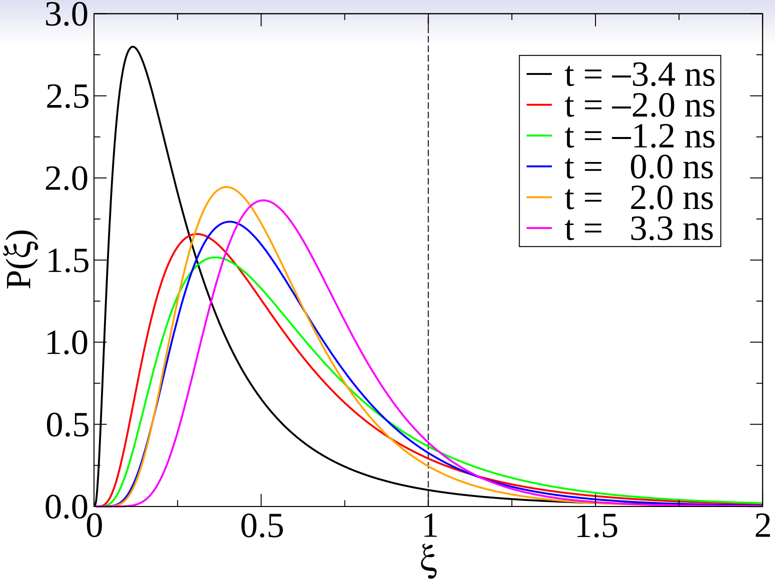

Is turbulence in this stagnating plasma isothermal?

Compare v_{flow} to a thermal conduction velocity (following [Zeldovich and Raizer, 1967]),

$$v_{\mathrm{cond}} = \frac{L_h}{\tau_{\mathrm{cond}}} \approx 4 \times 10^{21} \frac{\zeta(\langle Z_i \rangle)}{(\langle Z_i \rangle + 1)\lambda_{ei}} \frac{T^{5/2}}{n_e L_h},$$

where L_h is a length scale ($L_h \sim r_{\mathrm{pl}}$), λ_{ei} is the Coulomb logarithm, and $\zeta(8.5) \approx 2.7$; T is in units of eV, n_e in cm^{-3}, and L_h in cm.

When $v_{\mathrm{cond}}/v_{\mathrm{flow}} \gg 1$, isothermality is expected.

$v_{\mathrm{cond}}/v_{\mathrm{flow}} \sim 2$ for $L_h \sim r_{\mathrm{pl}}$ at $t = -3.4\,\mathrm{ns}$, and ~ 6 for later times.

An accurate determination of the degree of isothermality would require detailed simulations.The inferred T_e will also need to be reconsidered, since the emissivity depends on T_e strongly.

Interestingly, in Sandia Z experiments, where T_e and $\langle Z_i \rangle$ reach higher values, $v_{\mathrm{cond}}/v_{\mathrm{flow}} \gg 1$, thus the assumption of turbulence isothermality should be fully justified.